PHYSICS

Inducing ferromagnetism and Kondo effect in platinum by paramagnetic ionic gating

Lei Liang, Qihong Chen, Jianming Lu,* Wytse Talsma, Juan Shan, Graeme R. Blake, Thomas T. M. Palstra,† Jianting Ye‡

Electrically controllable magnetism, which requires the field-effect manipulation of both charge and spin degrees of freedom, has attracted growing interest since the emergence of spintronics. We report the reversible electrical switching of ferromagnetic (FM) states in platinum (Pt) thin films by introducing paramagnetic ionic liquid (PIL) as the gating media. The paramagnetic ionic gating controls the movement of ions with magnetic moments, which induces itinerant ferromagnetism on the surface of Pt films, with large coercivity and perpendicular anisotropy mimicking the ideal two-dimensional Ising-type FM state. The electrical transport of the induced FM state shows Kondo effect at low temperature, suggesting spatially separated coexistence of Kondo scattering beneath the FM interface. The tunable FM state indicates that paramagnetic ionic gating could serve as a versatile method to induce rich transport phenomena combining field effect and magnetism at PIL-gated interfaces.

INTRODUCTION

The ongoing quest to control magnetism by an electric field has attracted growing interest in both fundamental sciences and technological applications (*1*–*5*). In diluted magnetic semiconductors, switching magnetization can be achieved by modifying the density and type of carriers with external electric field (*1*, *5*–*7*). In multiferroic materials, the electric polarization can couple with the magnetization due to exchange striction effects (*8*–*10*). However, both aforementioned approaches require a strong electric field and usually reach magnetic ordering below room temperature, making them less feasible for applications. The materials showing high Curie temperatures (T_C) are generally metallic, which is difficult to manipulate by the field effect due to their intrinsically large carrier densities and, consequently, their short Thomas-Fermi screening lengths. The application of ionic liquids (ILs) on gating (Fig. 1A) has achieved inducing quantum phase transitions in many insulators (*11*–*13*) and semiconductors (*14*, *15*). A large number of carriers accumulated by ionic gating can even tune metallic devices (*2*, *16*–*19*). However, so far, ionic gating can only gradually vary metallic ferromagnetic (FM) materials (*2*, *3*, *17*), without realizing marked changes, such as ON/OFF switching of FM states.

Physically, the Stoner model of band ferromagnets explains spontaneous spin splitting in FM metals such as Fe, Co, and Ni, requiring the product of the density of states (DOS) at Fermi energy ρ_F and the exchange integral I larger than unity. Platinum (Pt) is normally regarded as an exchange-enhanced paramagnetic (PM) metal on the verge of FM instability. Hence, applying an electric field could induce the FM state in Pt if the enhanced product $I\rho_F$ satisfies the Stoner criterion, which might subsequently evoke marked changes in both magnetism and electrical transport. Meanwhile, decreasing the coordination number of the nearest neighboring atoms at the surface results in reduced electronic bandwidth (*20*). Consequently, ferromagnetism can be induced when the product of I and ρ_F is strongly enhanced by reducing dimensionality (*21*). For example, although not electrically controllable, the isolated Pt nanoparticles show ferromagnetism if their surfaces are perturbed by chemisorption (*22*).

Zernike Institute for Advanced Materials, University of Groningen, Nijenborgh 4, 9747 AG Groningen, Netherlands.
*Present address: State key laboratory for mesoscopic physics, Peking University, Beijing 100871, People's Republic of China.
†Present address: College van Bestuur, Universiteit Twente, 7500 AE Enschede, Netherlands.
‡Corresponding author. Email: j.ye@rug.nl

Despite the fact that ionic gating is capable of tuning a large number of carriers, it is highly demanding to realize the field-effect control of the spin degree of freedom. Here, paramagnetic ionic liquids (PILs), composed of anions containing transition metal with unpaired d orbitals, are introduced as gating media to induce magnetic interactions at the gated channel surface (Fig. 1B and see the Supplementary Materials). Therefore, it extends the conventional ionic gating to the spin tunability: the second intrinsic characteristic of the electron. Replacing the organic anions with metal complexes maintains the general physicochemical properties of ILs, such as low melting temperature (T_m < 200 K), negligible vapor pressure, and a large electrochemical window. Guided by these prerequisites that are crucial for ionic gating, butylmethylimidazolium tetrachloroferrate (BMIM[$FeCl_4$]) was synthesized for all experiments discussed below. All five 3d orbitals of Fe^{3+} in the anions are unpaired, giving a total spin quantum number of $S = 5/2$ (high-spin state). This PIL responds actively to external magnetic field even at room temperature (fig. S1). Magnetic susceptibility measurement shows that the PM BMIM[$FeCl_4$] has a large effective moment $\mu = 5.87\ \mu_B$, following Curie's law down to 2 K (fig. S2).

RESULTS

Gate-controllable electrical transport and field-induced ferromagnetism in Pt

Pt thin films with various thicknesses were prepared by magnetron sputtering. The films were patterned into Hall bar geometries and gated by BMIM[$FeCl_4$], as shown schematically in Fig. 1 (A to C). The gate voltage V_G dependence of the sheet resistance R_s (device A, thickness $t = 8.0$ nm) shows that the R_s can be reversibly controlled with negligible leak current I_G (Fig. 1D). The electrostatic nature of gating is further confirmed by a chronoamperometry experiment (fig. S3). According to ab initio calculation, the DOS peak of Pt lies slightly below the Fermi level (E_F) (*23*). Therefore, we expect that depleting carriers with negative V_G by driving the magnetic anions toward the Pt surface might satisfy the Stoner criterion; it would do this by increasing both ρ_F and I, due to the possible d-d interaction between Pt and $FeCl_4^-$. However, the negatively gated Pt maintains the PM state despite the increase of $|R_{xy}/B|$ (fig. S4). In contrast, FM states can be induced when the V_G dependence of the R_s shows an obvious drop at $V_G > 0$ (Fig. 1D), evidenced by the anomalous Hall effect (AHE) with clear hysteresis (Fig. 1E). This finding

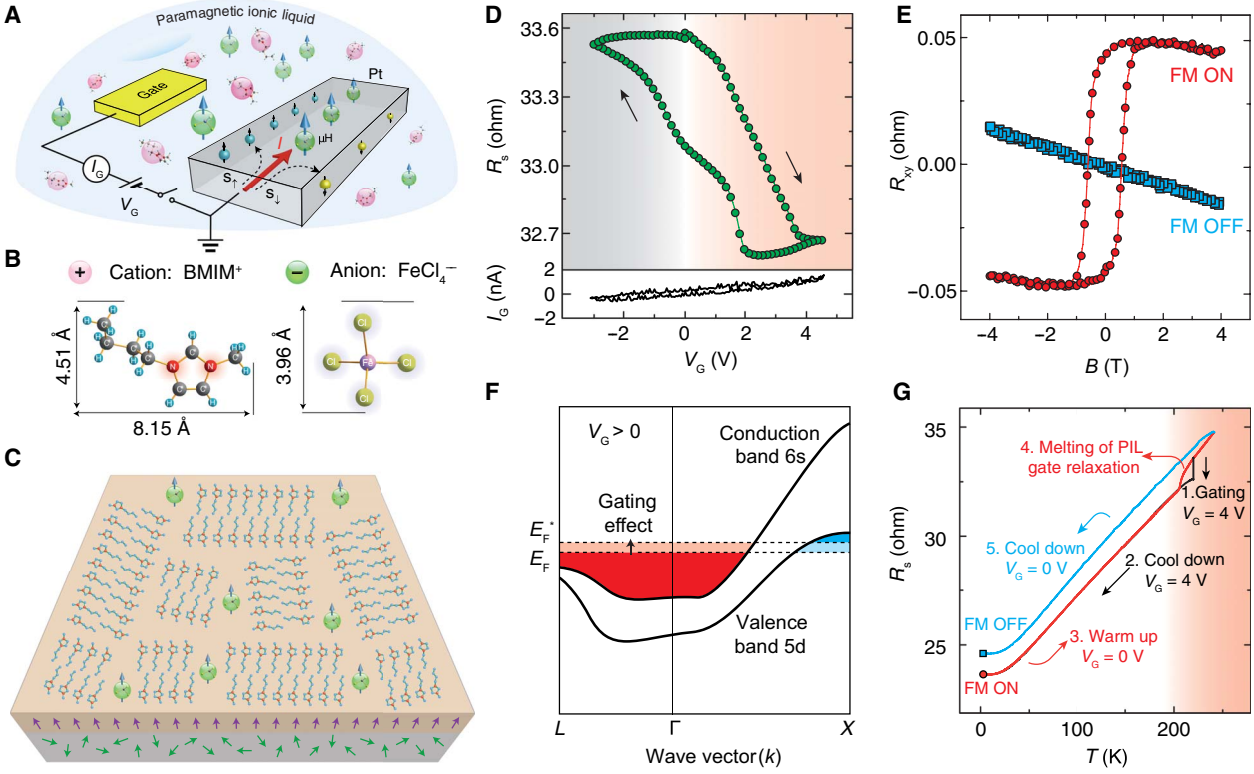

Fig. 1. Inducing ferromagnetism in Pt films by PIL gating. (**A**) Schematic diagram of PIL gating and transport measurement setup. The PIL is biased between a gold side gate electrode and the Pt channel. The cations and anions are illustrated as pink and green balls, respectively. (**B**) Composition of a typical PIL used in the measurement: $BMIM^+$ (cation) and $FeCl_4^-$ (anion). The size of the ions is determined from the single-crystal x-ray diffraction at 100 K. (**C**) Cations are driven toward the surface of Pt, forming ordered domain patterns after applying positive V_G, which leaves the domain interstitials filled with anions (*26*). The purple and green arrows denote the spin configuration of the surface and bulk Pt after PIL gating. (**D**) V_G dependence of R_s and corresponding I_G of device A (t = 8.0 nm, $-3\ V \leq V_G \leq 4\ V$, and sweeping rate of 50 mV/s). The reversible V_G dependence of R_s with linear I_G profile showing no signature of redox reaction indicates the electrostatic nature of gating. (**E**) R_{xy} measured at 2 K with/without applying V_G in accordance with the gating procedures in (G). The FM OFF and ON denote the linear Hall effect and the AHE (with hysteresis loop) observed in R_{xy} corresponding to the PM and FM states, respectively. (**F**) Field effect tuning of Fermi level E_F in the simplified band structure of Pt, where the Fermi surface of pristine Pt is composed of 5d and 6s states at X and Γ points of the Brillouin zone, respectively. Applying positive V_G lifts the E_F (to E_F^*), which changes the ratio between n_e and n_h of 6s and 5d band, respectively. (**G**) Magnetic states of Pt accompanied with five consecutive PIL gating procedures. AHE can be induced after cooling down with V_G = 4 V (E, red) corresponding to the FM ON state. Releasing the V_G at 2 K cannot remove the gating effect from the frozen ions. The R_s measured by warming the device from 2 to 260 K with V_G = 0 V (red) coincides with the cooling down curve (black) until 200 K. The melt of PIL at higher temperature releases the gating effect; hence, the R_s gradually increases with the redistribution of the accumulated ions. At 220 K, the R_s (red) shows identical value as the state before gating (black), indicating a repeatable gating process. Finally, cooling down the device from 260 to 2 K with V_G = 0 V (blue) shows linear Hall effect R_{xy} (E, blue dots) corresponding to the FM OFF state.

is consistent with other reports of the electric-field tuning of magnetic moments in systems with Stoner enhancement, where a positive V_G increases magnetic parameters such as saturation magnetization (M_s), coercivity (H_c), and T_C (*3*, *18*). This discrepancy between the experimental results and theoretical prediction suggests that the number of 5d electrons of Pt decreases when an electric field is applied in the direction of increasing the total number of electrons, mostly from the s band (*24*).

As reported in many other material systems (*11*, *12*), ionic gating can cause a significant change in carrier density due to its strong field effect. Here, the apparent carrier density measured by the Hall effect n_{Hall} (for example, extrapolated from R_{xy}/B) at 5 K significantly increases from $1.68 \times 10^{17}\ cm^{-2}$ to $3.24 \times 10^{17}\ cm^{-2}$ by applying $V_G = 4$ V (Fig. 1D). Because the actual change of carrier density is caused by the formation of electric double layer, the upper bound of the doping concentration can be simply determined by counting the number of ions accumulated at the channel surface. Direct imaging of the ion-gated Au surface by scanning tunneling microscopy (*25*) shows that the maximum induced carrier density is limited to $\sim 5 \times 10^{14}\ cm^{-2}$ (Fig. 1C). Therefore, the large discrepancy between the carrier density estimated from the surface ion concentration and the Hall effect indicates that n_{Hall} may not be a suitable indicator to quantify the actual change of carriers.

Despite the quantitative difference, large Δn_{Hall} implies substantial change of E_F, which is composed of the 6s electron–like and 5d hole–like pockets in open and nearly closed Fermi surfaces, respectively (Fig. 1F) (*26*–*28*). Positive V_G lifts E_F, accompanied by the increase of 6s electrons (n_e) and the decrease of 5d holes (n_h). Because of their opposite Hall coefficients, changes of n_e and n_h contribute destructively to the transverse resistance R_{xy} (*29*), causing seemingly large Δn_{Hall}. Because of the elevated E_F at $V_G > 0$, the conductivity improves by having more 6s electrons with higher mobility. The increase of E_F also reduces the available empty 5d states, causing less s-d scattering (*30*). Considering the intrinsically large carrier density in Pt and comparably small change of carriers caused by the field effect, observing large ΔR_s reflects the influence mainly by the reduced ratio of n_h/n_e. The FM state can be switched ON and OFF by following different sequences of PIL gating, as shown in Fig. 1G. The coincidence between the appearance of AHE and the decrease of R_s indicates a close relationship between the emergence of ferromagnetism and PIL gating.

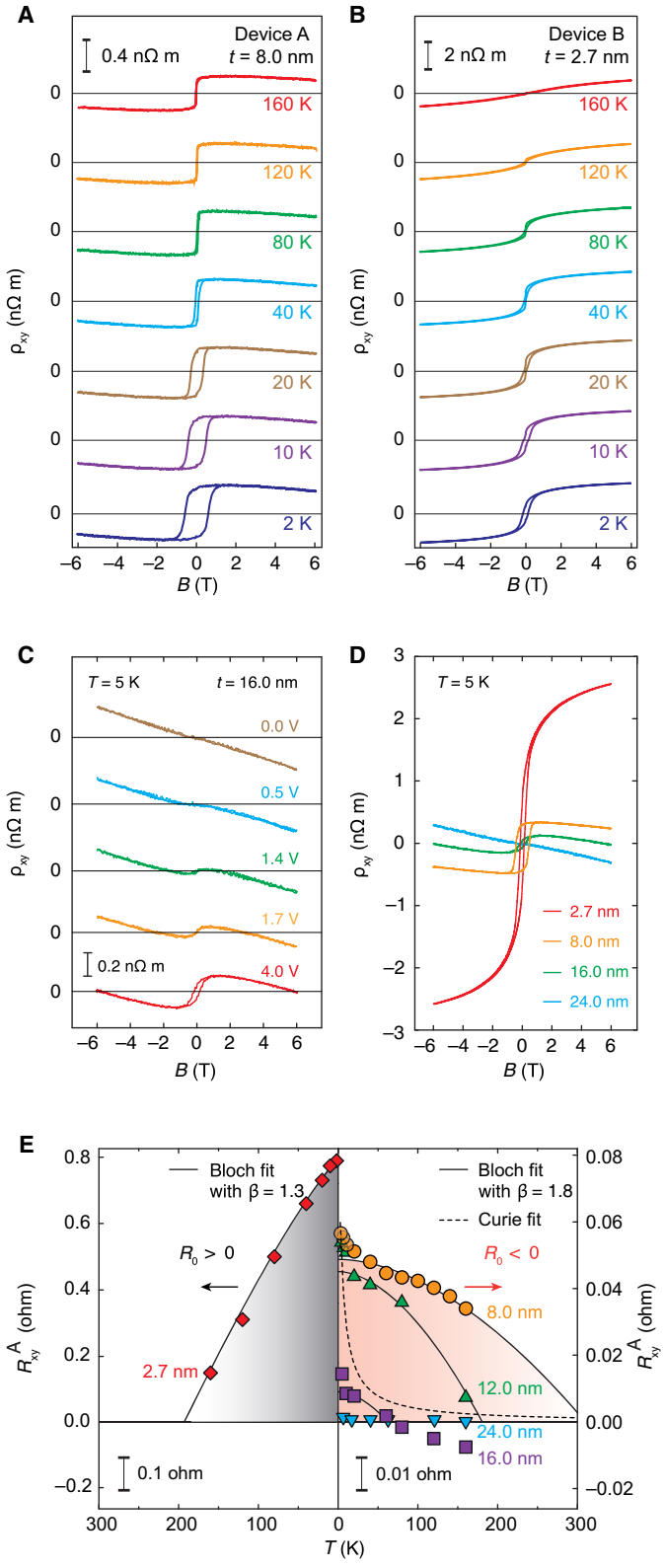

Fig. 2. Electrical transport of induced FM states after PIL gating. (**A** and **B**) Temperature variation of Hall resistivity ρ_{xy} for devices A (t = 8.0 nm) and B (t = 2.7 nm). (**C**) V_G variation of Hall resistivity ρ_{xy} for Pt film with t = 16 nm. (**D**) Thickness variation of the Hall resistivity ρ_{xy} for several Pt films. (**E**) Phase diagram of M_s (shown as R_{xy}^A) versus temperature for Pt films with different thicknesses.

The thickness dependence of AHE and magnetic phase diagram

For PIL-gated Pt films with two thicknesses t = 8.0 nm (device A) and 2.7 nm (device B), the temperature dependence of the Hall effect shows the occurrence of ferromagnetism manifested as AHE with clear hysteresis loops (Fig. 2, A and B). Empirically, the Hall resistivity in ferromagnets can be described by $\rho_{xy} = \rho_{xy}^0 + \rho_{xy}^A = R_0 B + R_A \mu_0 M$, where B is the magnetic field, M is the magnetization, and R_0 and R_A are the ordinary and anomalous Hall coefficients, respectively. Compared with device A, the anomalous Hall term ρ_{xy}^A in device B is one order of magnitude larger, suggesting stronger M in thinner films. It is worth noting that the strength of the induced FM states is closely linked to the V_G. As shown in Fig. 2C, the AHE measured for the same device at 5 K shows a gradual decrease of the ρ_{xy}^A and H_c after being cooled down with different V_G biases reduced from V_G = 4 V, which is consistent with the increase of R_0 demonstrated in Fig. 1F. Because of the strong screening in Pt, the field-induced modulation is confined beneath the surface within a depth of a few angstroms. The large hysteresis loop under the out-of-plane B field implies strong perpendicular magnetic anisotropy (PMA). Therefore, the induced FM state mimics the ideal two-dimensional itinerant Ising ferromagnetism. Magnetic films with PMA are highly pursued in spintronics, acting as the exchange bias layers in giant magnetoresistance devices (*31*) and magnetic tunnel junctions (*32*). The easily accessible PMA in PIL-gated Pt is technically favorable because of its electrical tunability.

It is well known that the induced FM state, demonstrated by the emerging hysteresis loop in AHE, should also leave traces in the longitudinal resistance. Surprisingly, the magnetoresistance (MR) shows a very weak signature of hysteresis loop, which is distinguishable only in the thinnest sample (t = 2.7 nm), when the influence of bulk Pt is minimal (fig. S5A). On the other hand, clear correspondence between the hysteretic MR and AHE was exhibited in PIL-gated palladium (Pd) film (fig. S6), which has an electronic structure very similar to Pt. The exact reason for this peculiarly small hysteresis in PIL-gated Pt might be related to the details of magnetic domain switching, where the R_s depends on the conductivity of domain walls formed during the magnetization reversal. For instance, anomalous change of MR has been observed in magnetically doped topological insulators (*33*), where more conductive hysteresis loops were observed in contrast to the conventional, more resistive loops.

As shown in Fig. 2D, the film thickness dependence of ρ_{xy} indicates that the ρ_{xy}^A increases with the decrease of t. For films with t > 24.0 nm, the AHE signal cannot be distinguished from the linear ρ_{xy} because the short screening length isolates the gating effect from affecting the bulk of gated Pt films, which remains PM with linear Hall response. With the increase of t, the enlarging bulk contribution acts as a short-circuit channel bypassing the topmost FM layer, resulting in the reduction of ρ_{xy}^A. Despite the larger ρ_{xy}^A in thinner films, the largest H_c was observed for t = 8.0 nm. Because the H_c is closely related to the formation of magnetic domains in different film morphologies, the optimization of the density and rigidity of domain walls at this intermediate thickness might give rise to the largest H_c.

The FM state is induced in Pt by the formation of an electric double layer, where the thickness is temperature-independent and expected to be a few angstrom thick due to the strong screening effect in a typical metal. We determine the R_{xy}^A by extracting the linear part of R_{xy} under high B field. The temperature dependence of the M_s (that is proportional to the R_{xy}^A) can be described by the Bloch equation $M_s(T) = M_s(0)(1 - CT^\beta)$, where $M_s(0)$ is the saturation magnetization at zero temperature and

C is a temperature-independent constant. The fittings for the high-temperature region ($T > 40$ K) yield β = 1.3 and 1.8 for the thinnest (t = 2.7 nm) and thicker films (t = 8.0, 12.0, and 16.0 nm), respectively (Fig. 2E). The similar β and resembling behavior of R_{xy}^{A} indicate that all FM samples with different thicknesses are likely originated from the same type of magnetization. In general, T_C decreases with the increase of t. For sample A (t = 8.0 nm) optimized for the largest H_c, the extrapolated T_C is even above the room temperature (300 K). The T_m of BMIM[$FeCl_4$] limits the upper-bound temperature of the induced FM state. Alternatively, choosing PILs with higher T_m might enable room temperature FM switching. At low temperature (<40 K), the M_s deviates from the Bloch equation, exhibiting an upturn in accordance with the $1/T$ dependence. This behavior signals the interaction between Pt and the PM $FeCl_4^-$ anions, whose PM magnetization significantly increases at low temperature, obeying Curie's law. It is worth noting that applying the same gating protocol to the identical Pt films using a conventional IL (fig. S7) shows no ferromagnetism despite the increased electrical conductivity (*19*). This clear difference indicates the importance of PIL in inducing the FM state in Pt.

The coexistence of Kondo effect and surface FM states

Depositing magnetic molecules on a metal film provides the ingredients essential to induce the Kondo effect, which has been observed in systems where a monolayer of a metal complex with unpaired spins is deposited on a gold (Au) film (*34*, *35*). The ionic gating has also been applied to study the Kondo effect (*36*, *37*). After cooling down the devices with positive V_G at which the R_s approaches saturation (Fig. 3A), systematically, we observed the R_s upturns below 20 K for all FM films with different thicknesses (Fig. 3B). The saturation of R_s toward zero temperature away from the linear dependence on ln(T) (inset of Fig. 3B) suggests the coexistence of the Kondo effect.

To quantitatively extract key parameters such as the Kondo resistance (R_K) and the Kondo temperature (T_K), we performed a numerical renormalization group (NRG) analysis (*38*), which normalizes the Kondo contribution to the transport by a universal parameter T/T_K. As shown in Fig. 3C, the $R_K(T)/R_K(0)$ dependences obtained for all measured films collapse into a single fitting curve as a function of T/T_K, which verifies the Kondo effect as the origin of the observed R_s upturns. As an example,

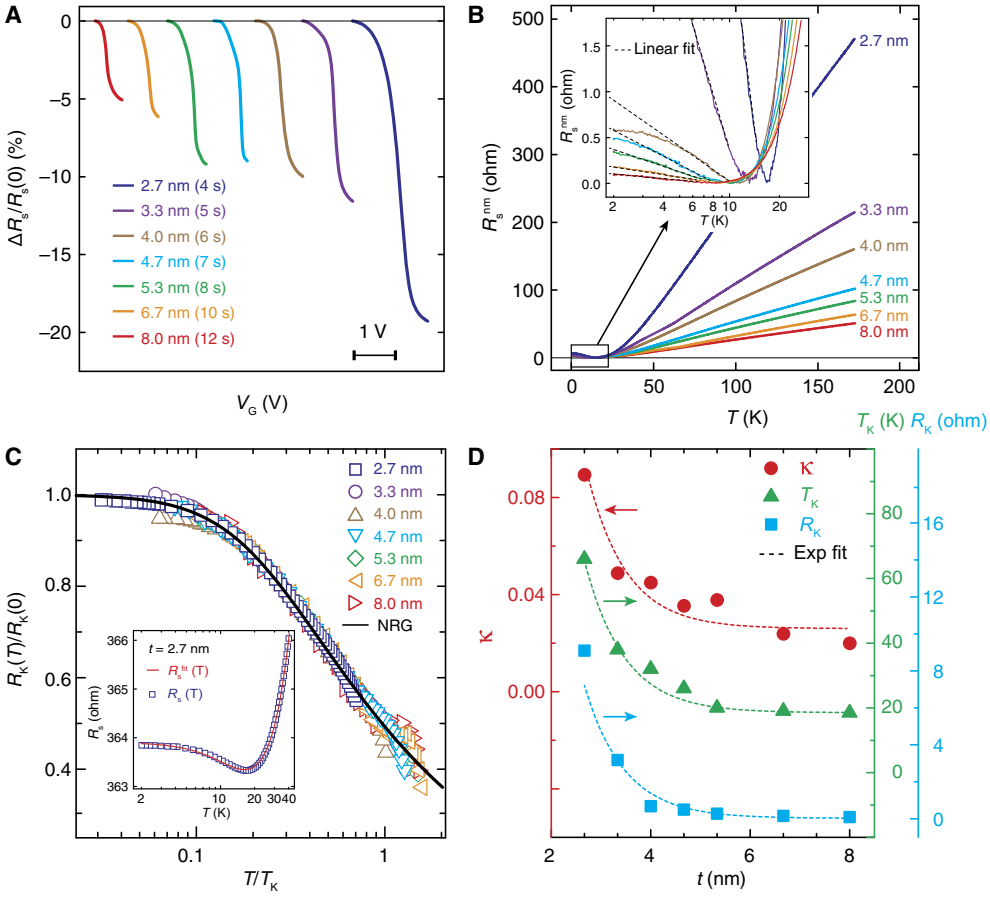

Fig. 3. Gate-induced Kondo effect in Pt films with different thicknesses. (**A**) V_G dependence of the R_s (T = 220 K) for a series of Pt films with different thicknesses (proportional to the sputtering time) showing the regime where the R_s rapidly decreases. (**B**) Temperature dependence of the R_s (V_G = 4 V) showing the Kondo effect in Pt films with different thicknesses. The R_s curves are normalized to the R_s measured at 150 K, according to $R_s^{nm}(T) = \frac{R_s(T)-R_s^{min}}{R_s(150\text{ K})-R_s^{min}} \times R_s(150\text{ K})$, where R_s^{min} is the minimum R_s of each curve. The inset shows the low temperature region, where the R_s^{nm} increases logarithmically with the decrease of T before reaching saturation. (**C**) Universal Kondo behavior observed for all gated Pt films (V_G = 4 V) showing that the normalized Kondo resistance $R_K(T)/R_K(0\text{ K})$ versus the reduced temperature T/T_K collapses into a single line, which can be described by the NRG method (black line). The inset shows an upturn in the temperature dependence of the R_s (t = 2.7 nm) observed from 2 to 30 K. The red line is the fitting from the NRG equation: $R_S(K) = R_0 + aT^b + R_K(T/T_K)$, where R_0 is the residual resistance, and a and b are temperature-independent coefficients. The empirical function $R_K(T/T_K)$ can be further expanded into $R_K(T/T_K) = R_K(0\text{ K})\left(\frac{T_K^2}{T^2+T_K^2}\right)^s$, where $R_K(0\text{ K})$ is the Kondo resistance at zero temperature, $T_K' = T_K/(2^{1/s}-1)^{1/2}$, and the parameter s is fixed to 0.225. (**D**) Thickness dependence of Kondo parameters R_K and T_K and effective thickness ratio κ. The dashed lines represent the exponential decay as a function of the film thickness t, where the decay constant c_0 = 0.8 is the same for all fittings.

a typical R_s upturn for t = 2.7 nm can be fitted well by the Kondo scenario (inset of Fig. 3C). When $T > T_K$, the increasing deviation from the NRG fitting is mainly attributed to the stronger phonon scattering.

Looking at the phenomenon of surface magnetization, the transport phenomena can be described by a simple model composed of two parallel conducting channels, where the ratio between the gate-tuned top layer and the total film thickness is denoted as $\kappa = t_{tp}/t$ (table S1). The estimated thickness of FM Pt is roughly equal to the topmost atomic layer t_{tp} (~2 Å). Both the gating-related parameter κ and Kondo parameters R_K and T_K decrease exponentially in the same trend as a function of t, indicating a close relationship between PIL gating and the induced Kondo effect (Fig. 3D). The narrowly confined FM state is in contrast with the much longer Kondo cloud length l_K (~5 nm) estimated by $l_K = \sqrt{\hbar D/k_B T_K}$, where k_B and $\hbar$ are the Boltzmann and reduced Planck's constant, respectively. Here, the diffusion constant D is given by $D = \frac{1}{3}\upsilon_F l_e$, where υ_F is the Fermi velocity and l_e is the elastic mean free path (*39*).

DISCUSSION

The origin of the AHE can be analyzed by scaling the anomalous Hall conductivity $\sigma_{AH} = \rho_{AH}/(\rho_{xx}^2 + \rho_{xy}^2)$ as a function of the longitudinal conductivity $\sigma_{xx} = \rho_{xx}/(\rho_{xx}^2 + \rho_{xy}^2)$ in a power law form as $\sigma_{AH} \propto \sigma_{xx}^{\gamma}$ (*40*). Figure 4 shows the scaling diagram of a comprehensive set of AHE data measured in different families of magnetic materials. In our experiment, the scaling of σ_{AH} is different from the asymmetric skew scattering from impurities ($\sigma_{AH} \propto \sigma_{xx}$) (*41*) and the side jump mechanism ($\sigma_{AH} \propto$ const.) (*42*). The fact that σ_{AH} appears to be independent of σ_{xx} implies that the induced ferromagnetism in Pt is of an intrinsic origin (*43*, *44*). For the PIL-induced FM state of Pt, the temperature

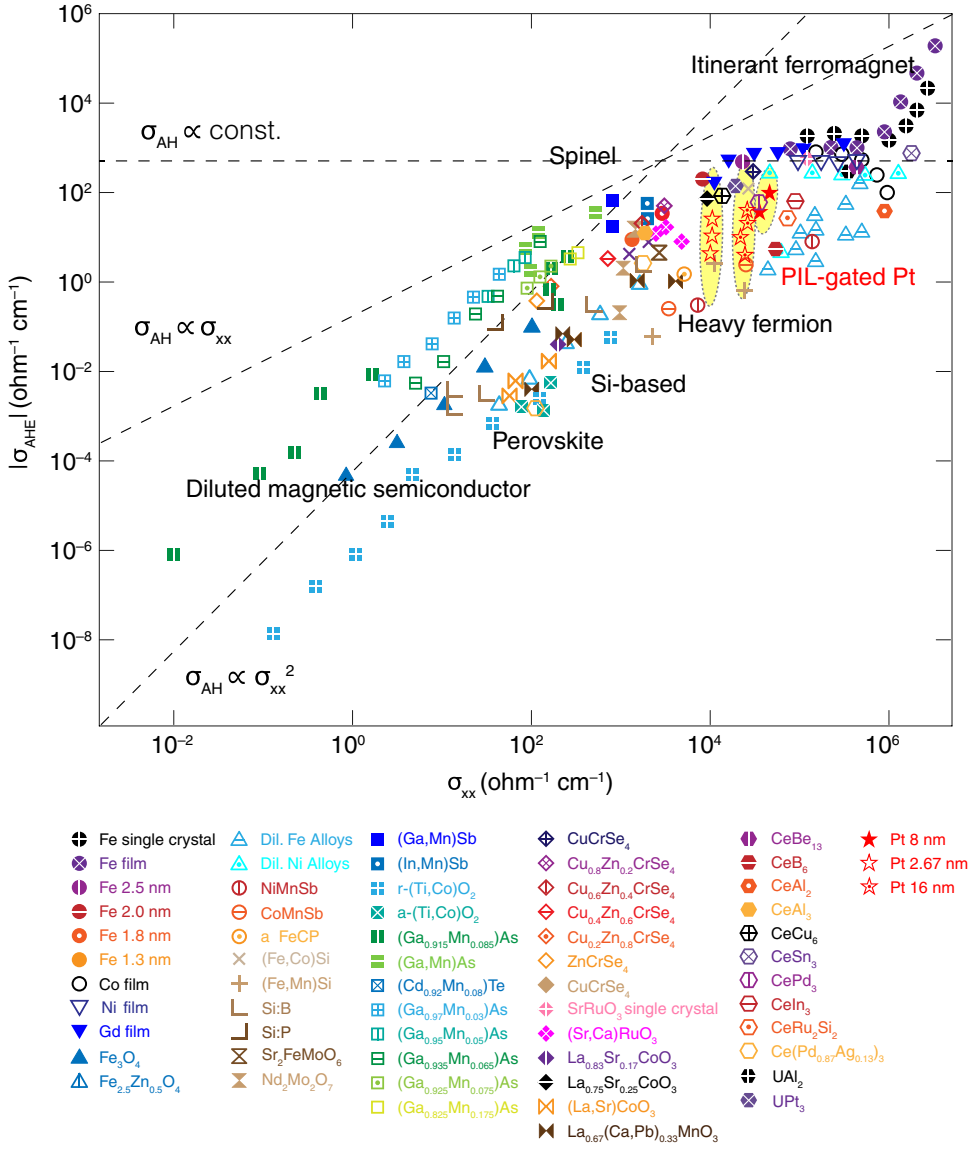

Fig. 4. Scaling diagram of AHE for PIL-gated Pt and various other magnetic systems. The AHE measured in PIL-gated Pt samples (shaded by yellow) are plotted together with other magnetic conductors reported previously (*53*–*56*), where each type of marker represents one material system. The σ_{AH} measured for the FM state of Pt shows weak dependence on the σ_{xx}.

dependence of σ_{AH} strongly relies on the applied V_G biases (Fig. 2C), which affects not only σ_{xx} but also σ_{AH}. The σ_{xx} of gated Pt film shows weak temperature dependence, whereas the σ_{AH} decreases significantly. These factors result in a large scaling exponent compared to other materials with $\gamma = 1$ and 2, which is also different from the behaviors observed in conventional itinerant ferromagnets (*45*). When Pt is deposited on a FM insulator, $Y_3Fe_5O_{12}$ (YIG), the AHE can be induced by the magnetic proximity effect (MPE) (*46*), showing similar sign reversal of the R_0 for $t < 3.0$ nm (*47*). We attributed this to the significant change of band structure at reduced dimensionality. In contrast to YIG, the strong Coulomb repulsion between anions in BMIM[$FeCl_4$] sets a large interionic distance, prohibiting FM exchange interaction. Hence, the PIL used in our gating remains PM down to 2 K (fig. S2), which firmly excludes MPE as the origin of the induced FM state.

Itinerant ferromagnetism is generally considered to be detrimental to the Kondo effect, whereas coexistence of FM and Kondo states has been observed in atomic contacts of pure itinerant ferromagnets (*48*) and heavy-fermion metals (*49*), where the coexistence is due to the local moments formed in a reduced coordinating environment and the itinerant-localized duality of f electrons, respectively. Although a comprehensive physical picture of the coexisting FM and Kondo states requires further study, the emerging ferromagnetism at the PIL/Pt interface likely originates from the d-d interaction between the 5d electrons perturbed by the field effect and the local magnetic moment of the metal halide anions. Although the FM state is confined at the PIL/Pt interface due to the strong screening, the spatially separated Kondo scattering extends deeper into the film, causing coexistence as two parallel channels.

To substantiate our observation that the induced FM state and Kondo effect in Pt films are caused by PIL gating, we performed a series of control experiments. By successively gating using different ionic media (IL-PIL-IL-PIL) on the same device (fig. S9), we firmly demonstrate the indispensable role of the PIL in inducing ferromagnetism. Compared with PIL-gated samples, the Pt film of the same thickness ($t = 8.0$ nm) with intentional Fe contamination underneath (nominal thickness, 0.2 nm) shows negligible AHE and H_c in the absence of the Kondo effect (fig. S5B). Moreover, the PIL-gated Au film maintains a PM state (fig. S10) because of its fully filled 5d band, whereas the Pd film yields a similar FM state after PIL gating (fig. S6). It is worth noting that although exclusive correlation has been demonstrated between PIL gating and the induced FM state, the exact carrier doping mechanism might not be limited to the electrostatic effect. Consistent with the fully reversible and repeatable behaviors shown in the control experiments (fig. S9), the reversible, electrochemically induced phase transformation that is stabilized by gating can be the alternative doping mechanism (*50*). Therefore, probing the redox states of the gated surface would help in resolving the exact doping mechanism (*51*). Our present results of inducing FM states reveal the universality of PIL gating in switching magnetism, which will benefit the development of spintronic devices that can simultaneously control charge and spin degrees of freedom.

MATERIALS AND METHODS

Synthesis of PILs

A series of PILs (fig. S1A) were synthesized by mixing stoichiometric amounts of solid organic-based halides and anhydrous transition metal halides (Sigma-Aldrich) inside a N_2-filled glove box (*52*). The ratios of the two components were calculated based on the selection of the corresponding metal chlorides, taking the oxidation states of the metal ions (for example, 3+ and 2+) and the coordination number of the corresponding metal complex (for example, MR_4 and MR_6) into account. For example, to synthesize BMIM[$FeCl_4$], which was later chosen for all transport measurements, BMIM[Cl]/anhydrous $FeCl_3$ precursors with a molar ratio of 1.05:1 were chosen to ensure that all Fe elements contained in the PIL could stay in the form of $FeCl_4^-$. The mixture was dispersed in dichloromethane by stirring overnight at room temperature to form the PIL. The dichloromethane solvent and other volatile residual impurities in the PIL were removed by a rotary vacuum evaporator ($P < 10^{-3}$ mbar). The as-prepared BMIM[$FeCl_4$] shows a strong response to a magnet even at room temperature (fig. S1B).

Single-crystal x-ray diffraction

The crystal structures of PIL were determined by x-ray diffraction using a Bruker D8 Venture diffractometer equipped with a monochromator (Triumph) and an area detector (Photon 100). We used Mo K_α radiation and carried out the measurement at 100 K to minimize the thermal vibrations. The PIL crystals were picked up using nylon loop with cryo-oil and cooled using a nitrogen flow (Cryostream Plus, Oxford Cryosystems). The diffraction data were processed using the Bruker Apex II software. The crystal structures were solved and refined using the SHELXTL software.

Device fabrication

Transistor devices used for PIL gating were all fabricated by standard microfabrication. Using electron beam lithography, we defined the Hall bar at $3 \times 7\ \mu m^2$. All metal channels (Pt, Pd, and Au) were prepared by dc magnetron sputtering (Kurt J. Lesker) after pumping the chamber below 1.0×10^{-8} mbar. Sputtering powers (50 to 200 W) and duration (2 to 12 s) were optimized to prepare films with different thicknesses. Separately, contact electrodes comprising bilayer Ti/Au (5/70 nm) were deposited onto the patterned Hall bars using e-beam evaporation (FC-2000, Temescal) below 1.0×10^{-6} mbar. Afterward, an Al_2O_3 isolation layer (30 nm) was deposited to cover contact electrodes, limiting the gating effect to only the exposed channel surface.

Electrical transport measurement

Low-temperature electrical transports were measured in a helium cryostat (Physical Property Measurement System, Quantum Design) under out-of-plane magnetic fields up to 6 T. All transport properties were measured by two lock-in amplifiers (SR830, Stanford Research) using a constant ac current excitation of 50 μA at 13.367 Hz. The voltage bias on BMIM[$FeCl_4$] (the PIL used in all gating experiments) was applied by a source measure unit (model 2450, Keithley).

Magnetic property characterization

The magnetization curves of BMIM[$FeCl_4$] were measured in a SQUID magnetometer (MPMS XL-7, Quantum Design) up to 7 T. The temperature dependence of magnetic susceptibility was measured using zero-field cooling (ZFC) and field cooling (FC) methods. In the ZFC method, the sample was first cooled down to 2 K in zero field and measured during warming up in a field of 100 Oe. In the FC method, the measurement procedure was identical except that PIL was first cooled down in a field of 2 T.

SUPPLEMENTARY MATERIALS

Supplementary material for this article is available at http://advances.sciencemag.org/cgi/content/full/4/4/eaar2030/DC1

section S1. Magnetization and magnetic susceptibility measurement

REFERENCES AND NOTES

1. H. Ohno, D. Chiba, F. Matsukura, T. Omiya, E. Abe, T. Dietl, Y. Ohno, K. Ohtani, Electric-field control of ferromagnetism. *Nature* **408**, 944–946 (2000).
2. M. Weisheit, S. Fähler, A. Marty, Y. Souche, C. Poinsignon, D. Givord, Electric field-induced modification of magnetism in thin-film ferromagnets. *Science* **315**, 349–351 (2007).
3. D. Chiba, S. Fukami, K. Shimamura, N. Ishiwata, K. Kobayashi, T. Ono, Electrical control of the ferromagnetic phase transition in cobalt at room temperature. *Nat. Mater.* **10**, 853–856 (2011).
4. F. Matsukura, Y. Tokura, H. Ohno, Control of magnetism by electric fields. *Nat. Nanotechnol.* **10**, 209–220 (2015).
5. D. Chiba, M. Yamanouchi, F. Matsukura, H. Ohno, Electrical manipulation of magnetization reversal in a ferromagnetic semiconductor. *Science* **301**, 943–945 (2003).
6. Y. Yamada, K. Ueno, T. Fukumura, H. T. Yuan, H. Shimotani, Y. Iwasa, L. Gu, S. Tsukimoto, Y. Ikuhara, M. Kawasaki, Electrically induced ferromagnetism at room temperature in cobalt-doped titanium dioxide. *Science* **332**, 1065–1067 (2011).
7. T. Dietl, A ten-year perspective on dilute magnetic semiconductors and oxides. *Nat. Mater.* **9**, 965–974 (2010).
8. T. Kimura, T. Goto, H. Shintani, K. Ishizaka, T. Arima, Y. Tokura, Magnetic control of ferroelectric polarization. *Nature* **426**, 55–58 (2003).
9. W. Eerenstein, N. D. Mathur, J. F. Scott, Multiferroic and magnetoelectric materials. *Nature* **442**, 759–765 (2006).
10. S.-W. Cheong, M. Mostovoy, Multiferroics: A magnetic twist for ferroelectricity. *Nat. Mater.* **6**, 13–20 (2007).
11. J. T. Ye, S. Inoue, K. Kobayashi, Y. Kasahara, H. T. Yuan, H. Shimotani, Y. Iwasa, Liquid-gated interface superconductivity on an atomically flat film. *Nat. Mater.* **9**, 125–128 (2010).
12. J. T. Ye, Y. J. Zhang, R. Akashi, M. S. Bahramy, R. Arita, Y. Iwasa, Superconducting dome in a gate-tuned band insulator. *Science* **338**, 1193–1196 (2012).
13. J. M. Lu, O. Zheliuk, I. Leermakers, N. F. Q. Yuan, U. Zeitler, K. T. Law, J. T. Ye, Evidence for two-dimensional Ising superconductivity in gated MoS_2. *Science* **350**, 1353–1357 (2015).
14. Y. J. Zhang, T. Oka, R. Suzuki, J. T. Ye, Y. Iwasa, Electrically switchable chiral light-emitting transistor. *Science* **344**, 725–728 (2014).
15. Q. H. Wang, K. Kalantar-Zadeh, A. Kis, J. N. Coleman, M. S. Strano, Electronics and optoelectronics of two-dimensional transition metal dichalcogenides. *Nat. Nanotechnol.* **7**, 699–712 (2012).
16. T. Maruyama, Y. Shiota, T. Nozaki, K. Ohta, N. Toda, M. Mizuguchi, A. A. Tulapurkar, T. Shinjo, M. Shiraishi, S. Mizukami, Y. Ando, Y. Suzuki, Large voltage-induced magnetic anisotropy change in a few atomic layers of iron. *Nat. Nanotechnol.* **4**, 158–161 (2009).
17. K. Shimamura, D. Chiba, S. Ono, S. Fukami, N. Ishiwata, M. Kawaguchi, K. Kobayashi, T. Ono, Electrical control of Curie temperature in cobalt using an ionic liquid film. *Appl. Phys. Lett.* **100**, 122402 (2012).
18. A. Obinata, Y. Hibino, D. Hayakawa, T. Koyama, K. Miwa, S. Ono, D. Chiba, Electric-field control of magnetic moment in Pd. *Sci. Rep.* **5**, 14303 (2015).
19. S. Shimizu, K. S. Takahashi, T. Hatano, M. Kawasaki, Y. Tokura, Y. Iwasa, Electrically tunable anomalous Hall effect in Pt thin films. *Phys. Rev. Lett.* **111**, 216803 (2013).
20. C. Binns, *Nanomagnetism: Fundamentals and Applications* (Elsevier, 2014), 328 pp.
21. S. Sakuragi, T. Sakai, S. Urata, S. Aihara, A. Shinto, H. Kageshima, M. Sawada, H. Namatame, M. Taniguchi, T. Sato, Thickness-dependent appearance of ferromagnetism in Pd(100) ultrathin films. *Phys. Rev. B* **90**, 054411 (2014).
22. Y. Sakamoto, Y. Oba, H. Maki, M. Suda, Y. Einaga, T. Sato, M. Mizumaki, N. Kawamura, M. Suzuki, Ferromagnetism of Pt nanoparticles induced by surface chemisorption. *Phys. Rev. B* **83**, 104420 (2011).
23. A. H. MacDonald, J. M. Daams, S. H. Vosko, D. D. Koelling, Influence of relativistic contributions to the effective potential on the electronic structure of Pd and Pt. *Phys. Rev. B* **23**, 6377–6398 (1981).
24. M. Oba, K. Nakamura, T. Akiyama, T. Ito, M. Weinert, A. J. Freeman, Electric-field-induced modification of the magnon energy, exchange interaction, and curie temperature of transition-metal thin films. *Phys. Rev. Lett.* **114**, 107202 (2015).
25. Y. Z. Su, Y. C. Fu, J. W. Yan, Z. B. Chen, B. W. Mao, Double layer of Au(100)/ionic liquid interface and its stability in imidazolium-based ionic liquids. *Angew. Chem. Int. Ed. Engl.* **48**, 5148–5151 (2009).
26. L. R. Windmiller, J. B. Ketterson, S. Hornfeldt, Experimental determination of the Fermi radius, velocity, and g factor in Pd and Pt. *J. Appl. Phys.* **40**, 1291 (1969).
27. O. K. Andersen, Electronic structure of the fcc transition metals Ir, Rh, Pt, and Pd. *Phys. Rev. B* **2**, 883–906 (1970).
28. G. Fischer, H. Hoffmann, J. Vancea, Mean free path and density of conductance electrons in platinum determined by the size effect in extremely thin films. *Phys. Rev. B* **22**, 6065–6073 (1980).
29. V. L. Moruzzi, J. F. Janak, A. R. Williams, *Calculated Electronic Properties of Metals* (Elsevier, 2013), 196 pp.
30. M. Sagmeister, U. Brossmann, S. Landgraf, R. Würschum, Electrically tunable resistance of a metal. *Phys. Rev. Lett.* **96**, 156601 (2006).
31. S. Maat, K. Takano, S. Parkin, E. E. Fullerton, Perpendicular exchange bias of Co/Pt multilayers. *Phys. Rev. Lett.* **87**, 087202 (2001).
32. S. Ikeda, K. Miura, H. Yamamoto, K. Mizunuma, H. D. Gan, M. Endo, S. Kanai, J. Hayakawa, F. Matsukura, H. Ohno, A perpendicular-anisotropy CoFeB–MgO magnetic tunnel junction. *Nat. Mater.* **9**, 721–724 (2010).
33. J. G. Checkelsky, J. Ye, Y. Onose, Y. Iwasa, Y. Tokura, Dirac-fermion-mediated ferromagnetism in a topological insulator. *Nat. Phys.* **8**, 729–733 (2012).
34. T. Gang, M. D. Yilmaz, D. Ataç, S. K. Bose, E. Strambini, A. H. Velders, M. P. de Jong, J. Huskens, W. G. van der Wiel, Tunable doping of a metal with molecular spins. *Nat. Nanotechnol.* **7**, 232–236 (2012).
35. A. Zhao, Q. Li, L. Chen, H. Xiang, W. Wang, S. Pan, B. Wang, X. Xiao, J. Yang, J. G. Hou, Q. Zhu, Controlling the Kondo effect of an adsorbed magnetic ion through its chemical bonding. *Science* **309**, 1542–1544 (2005).
36. M. Lee, J. R. Williams, S. Zhang, C. D. Frisbie, D. Goldhaber-Gordon, Electrolyte gate-controlled Kondo effect in $SrTiO_3$. *Phys. Rev. Lett.* **107**, 256601 (2011).
37. Y. Li, R. Deng, W. Lin, Y. Tian, H. Peng, J. Yi, B. Yao, T. Wu, Electrostatic tuning of Kondo effect in a rare-earth-doped wide-band-gap oxide. *Phys. Rev. B* **87**, 155151 (2013).
38. R. Bulla, T. A. Costi, T. Pruschke, Numerical renormalization group method for quantum impurity systems. *Rev. Mod. Phys.* **80**, 395–450 (2008).
39. V. Chandrasekhar, C. Van Haesendonck, A. Zawadowski, *Kondo Effect and Dephasing in Low-Dimensional Metallic Systems* (Springer Science & Business Media, 2001), 265 pp.
40. N. Nagaosa, J. Sinova, S. Onoda, A. H. MacDonald, N. P. Ong, Anomalous Hall effect. *Rev. Mod. Phys.* **82**, 1539–1592 (2010).
41. J. Smit, The spontaneous hall effect in ferromagnetics I. *Physica* **21**, 877–887 (1955).
42. L. Berger, Side-jump mechanism for the Hall effect of ferromagnets. *Phys. Rev. B* **2**, 4559–4566 (1970).
43. J. M. Luttinger, Theory of the Hall effect in ferromagnetic substances. *Phys. Rev.* **112**, 739–751 (1958).
44. N. Nagaosa, Anomalous Hall effect—A new perspective. *J. Phys. Soc. Jpn.* **75**, 042001 (2006).
45. T. Miyasato, N. Abe, T. Fujii, A. Asamitsu, S. Onoda, Y. Onose, N. Nagaosa, Y. Tokura, Crossover behavior of the anomalous Hall effect and anomalous Nernst effect in itinerant ferromagnets. *Phys. Rev. Lett.* **99**, 086602 (2007).
46. Y. M. Lu, Y. Choi, C. M. Ortega, X. M. Cheng, J. W. Cai, S. Y. Huang, L. Sun, C. L. Chien, Pt magnetic polarization on $Y_3Fe_5O_{12}$ and magnetotransport characteristics. *Phys. Rev. Lett.* **110**, 147207 (2013).
47. S. Meyer, R. Schlitz, S. Geprägs, M. Opel, H. Huebl, R. Gross, S. T. B. Goennenwein, Anomalous Hall effect in YIG|Pt bilayers. *Appl. Phys. Lett.* **106**, 132402 (2015).
48. M. R. Calvo, J. Fernández-Rossier, J. J. Palacios, D. Jacob, D. Natelson, C. Untiedt, The Kondo effect in ferromagnetic atomic contacts. *Nature* **458**, 1150–1153 (2009).
49. F. Steglich, J. Arndt, O. Stockert, S. Friedemann, M. Brando, C. Klingner, C. Krellner, C. Geibel, S. Wirth, S. Kirchner, Q. Si, Magnetism, f-electron localization and superconductivity in 122-type heavy-fermion metals. *J. Phys. Condens. Matter* **24**, 294201 (2012).
50. N. Lu, P. Zhang, Q. Zhang, R. Qiao, Q. He, H.-B. Li, Y. Wang, J. Guo, D. Zhang, Z. Duan, Z. Li, M. Wang, S. Yang, M. Yan, E. Arenholz, S. Zhou, W. Yang, L. Gu, C.-W. Nan, J. Wu, Y. Tokura,

P. Yu, Electric-field control of tri-state phase transformation with a selective dual-ion switch. *Nature* **546**, 124–128 (2017).
51. T. A. Petach, M. Lee, R. C. Davis, A. Mehta, D. Goldhaber-Gordon, Mechanism for the large conductance modulation in electrolyte-gated thin gold films. *Phys. Rev. B* **90**, 081108 (2014).
52. S. Hayashi, H.-o. Hamaguchi, Discovery of a magnetic ionic liquid [Bmim]$FeCl_4$. *Chem. Lett.* **33**, 1590–1591 (2004).
53. H. Toyosaki, T. Fukumura, Y. Yamada, K. Nakajima, T. Chikyow, T. Hasegawa, H. Koinuma, M. Kawasaki, Anomalous Hall effect governed by electron doping in a room-temperature transparent ferromagnetic semiconductor. *Nat. Mater.* **3**, 221–224 (2004).
54. N. Manyala, Y. Sidis, J. F. DiTusa, G. Aeppli, D. P. Young, Z. Fisk, Large anomalous Hall effect in a silicon-based magnetic semiconductor. *Nat. Mater.* **3**, 255–262 (2004).
55. T. Fukumura, H. Toyosaki, K. Ueno, M. Nakano, T. Yamasaki, M. Kawasaki, A scaling relation of anomalous Hall effect in ferromagnetic semiconductors and metals. *Jpn. J. Appl. Phys.* **46**, L642 (2007).
56. D. Chiba, A. Werpachowska, M. Endo, Y. Nishitani, F. Matsukura, T. Dietl, H. Ohno, Anomalous Hall effect in field-effect structures of (Ga,Mn)As. *Phys. Rev. Lett.* **104**, 106601 (2010).
57. R. E. Del Sesto, T. M. McCleskey, A. K. Burrell, G. A. Baker, J. D. Thompson, B. L. Scott, J. S. Wilkes, P. Williams, Structure and magnetic behavior of transition metal based ionic liquids. *Chem. Commun.* **0**, 447–449 (2008).
58. H. Nakayama, J. Ye, T. Ohtani, Y. Fujikawa, K. Ando, Y. Iwasa, E. Saitoh, Electroresistance effect in gold thin film induced by ionic-liquid-gated electric double layer. *Appl. Phys. Express* **5**, 023002 (2012).
59. G. M. Minkov, O. E. Rut, A. V. Germanenko, A. A. Sherstobitov, V. I. Shashkin, O. I. Khrykin, V. M. Daniltsev, Quantum corrections to the conductivity in two-dimensional systems: Agreement between theory and experiment. *Phys. Rev. B* **64**, 235327 (2001).
60. W. Niu, M. Gao, X. Wang, F. Song, J. Du, X. Wang, Y. Xu, R. Zhang, Evidence of weak localization in quantum interference effects observed in epitaxial $La_{0.7}Sr_{0.3}MnO_3$ ultrathin films. *Sci. Rep.* **6**, 26081 (2016).
61. L. J. Zhu, S. H. Nie, P. Xiong, P. Schlottmann, J. H. Zhao, Orbital two-channel Kondo effect in epitaxial ferromagnetic $L1_0$-MnAl films. *Nat. Commun.* **7**, 10817 (2016).
62. M. Kobayashi, K. Tanaka, A. Fujimori, S. Ray, D. D. Sarma, Critical test for Altshuler-Aronov theory: Evolution of the density of states singularity in double perovskite Sr_2FeMoO_6 with controlled disorder. *Phys. Rev. Lett.* **98**, 246401 (2007).

Acknowledgments: We thank B. J. van Wees and G. E. W. Bauer for fruitful discussion. **Funding:** The work was supported by the European Research Council (consolidator grant no. 648855 Ig-QPD) and Dutch national facility NanoLabNL. L.L. was supported by the Ubbo Emmius scholarship of University of Groningen. **Author contributions:** J.Y. and L.L. conceived the experiments. L.L. and W.T. fabricated the devices. L.L. designed and carried out the transport experiments, with help from Q.C. and J.L. J.S., L.L., G.R.B., and T.T.M.P. measured the crystallographic and magnetic properties. J.Y., L.L., and T.T.M.P. constructed the theory. All authors were involved in the data analysis. L.L. and J.Y. wrote the manuscript, with the help of co-authors. **Competing interests:** The authors declare that they have no competing interests. **Data and materials availability:** All data needed to evaluate the conclusions in the paper are present in the paper and/or the Supplementary Materials. Additional data related to this paper may be requested from the authors.

Submitted 12 October 2017
Accepted 16 February 2018
Published 6 April 2018
10.1126/sciadv.aar2030

Citation: L. Liang, Q. Chen, J. Lu, W. Talsma, J. Shan, G. R. Blake, T. T. M. Palstra, J. Ye, Inducing ferromagnetism and Kondo effect in platinum by paramagnetic ionic gating. *Sci. Adv.* **4**, eaar2030 (2018).